Surface & Coatings Technology 423 (2021) 127585

Contents lists available at ScienceDirect

Surface & Coatings Technology

journal homepage: www.elsevier.com/locate/surfcoat

Influence of nozzle configuration and particle size on characteristics and sliding wear behaviour of HVAF-sprayed WC-CoCr coatings

Kaveh Torkashvand [a,*], Mohit Gupta [a], Stefan Björklund [a], Francesco Marra [b], Lidia Baiamonte [a,b], Shrikant Joshi [a]

[a] Department of Engineering Science, University West, Sweden
[b] Department of Chemical Engineering Materials Environment, Sapienza University of Rome, Italy

ARTICLE INFO

Keywords:
Particle size
Nozzle configuration
HVAF
WC-CoCr
Sliding wear

ABSTRACT

In this study, effect of feedstock particle size and nozzle configuration on deposition, microstructural features, hardness and sliding wear behaviour of high velocity air fuel (HVAF)-sprayed WC-CoCr coatings was evaluated. Three different WC-CoCr powders with nominal particle sizes of 5/20 μm (fine), 5/30 μm (medium) and 15/45 μm (coarse) were sprayed employing a HVAF gun with four distinct DeLaval nozzle configurations involving different lengths and/or exit diameters. Microstructure, phase constitution and mechanical characteristics of the coatings were evaluated using SEM, EDS, XRD and micro indentation testing. Specific wear rate for all the samples was determined under sliding conditions and a comprehensive post wear analysis was conducted. X-ray diffraction analysis showed negligible decarburization in all the HVAF-sprayed coatings. It was shown that decrease in particle size of employed feedstock results in discernible changes in microstructural features of the coatings as well as considerable improvement in their performance. Also, notable changes in wear mechanisms were identified on reducing particle size from coarse to medium or fine. Fine and coarse feedstock powders were found to be sensitive to the type of nozzle used while no major difference was observed in coatings from powders with medium cut size sprayed with different nozzles.

1. Introduction

High velocity air-fuel (HVAF) spraying method has been considered increasingly attractive for spraying WC-based wear resistant coatings and attracting significant research attention. This is largely by virtue of its capability to produce high quality coatings and overcoming some of the existing problems such as decarburization [1–3]. HVAF spraying method typically generates higher particle velocities leading to higher kinetic energy and, due to the lower flame temperature, the particle temperatures are also lower compared to other spraying techniques like high velocity oxy-fuel (HVOF). The latter is a key factor responsible for diminishing decarburization [4,5]. Moreover, in the HVAF method, substituting air in place of oxygen not only results in lower spraying costs, but can also effectively mitigate oxidation of the feedstock. Consequently, a finer powder cut size can be used as feedstock [6–8]. However, different hardware configurations in the HVAF method result in varied particle temperatures and velocities. Different torch configurations can be achieved particularly through variations in length and the convergent-divergent design of the nozzles. Therefore, selecting a proper configuration demands a deep understanding of its effect on properties of the resultant coating. Feedstock characteristics such as morphology, density, and particles size also significantly influence the resultant coating properties. Among these, the particle size distribution can be considered a prominent feedstock characteristic for a given chemistry in case of HVAF spraying. Both the temperature and velocity attained in flight by particles are strongly dependent on their size, which is also a determining factor in selecting the most appropriate HVAF spraying configuration [9,10].

Some investigations have been previously conducted to study the effect of HVAF process parameters on characteristics and performance of WC-based coatings. Matikainen et al. [11] studied the effect of nozzle configuration on tribological properties of HVAF-sprayed WC-CoCr coatings deposited using feedstock powder of 10–30 μm size range. They employed a M3 gun (Uniquecoat Technologies LLC, USA) and utilized three nozzles of the same length but with different exit diameters: one cylindrical (named 4L0) and two convergent-divergent configurations

* Corresponding author.
E-mail address: Kaveh.torkashvand@hv.se (K. Torkashvand).

https://doi.org/10.1016/j.surfcoat.2021.127585
Received 16 April 2021; Received in revised form 29 July 2021; Accepted 30 July 2021
Available online 5 August 2021

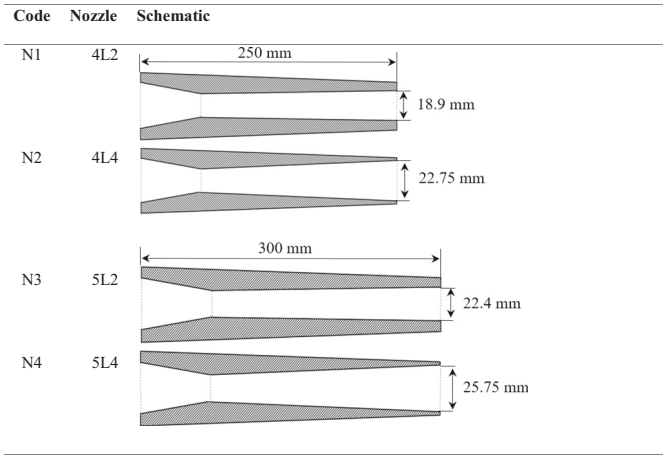

Fig. 1. Different nozzle configurations used for spraying.

(named 4L2 and 4L4) with increasing exit diameter as the nozzle designation changes from 4L0 to 4L2 and 4L4 (see Fig. 1 for 4L2 and 4L4 designs). Their results showed that average particle velocity can rise from 780 m·s^{-1} for a straight bore nozzle to 900 m·s^{-1} for a convergent-divergent nozzle, resulting in substantial improvement in density and microstructure of the coating. Lyphout et al. [12], utilizing an identical gun with different nozzles varying in length to spray an identical powder, studied mechanical and wear properties of WC-CoCr coatings. Their results showed that increasing length of the nozzle leads to an improvement in microhardness and abrasion wear resistance of the coating. In another study by Kumar et al. [10], it was shown that the AK06 HVAF gun (Kermetico, USA) with three different nozzle designations 5O, 5E and 5L, of varying geometrical design, can result in average particle velocities of 1010, 960 and 895 m·s^{-1}, respectively, when spraying WC-CoCr feedstock powder of the same particle size (20–45 μm). However, the above investigations were conducted on powders with an identical particle size and, as a result, do not provide a broad view of how the nozzle geometry-particle size combinations can influence the properties and performance of the resultant coatings. Besides, given the fact that HVAF parameters are primarily hardware dependent [12] as compared to other spraying techniques like HVOF and plasma spraying where other spray variables can play a major role [13,14], changing nozzles covers a wide-ranging process window in HVAF spraying and is of considerable practical relevance. Consequently, considering the rapid progress of the HVAF technology and commercial availability of different spray equipment, the influence of nozzle configuration needs to be well established for different powder particle sizes to be sprayed.

During the spraying process, particles attain different temperatures and velocities depending on their size. Another key factor is the duration of high temperature exposure, which itself is dependent on the size (mass) of the particles [15,16] since the in-flight residence time is governed by the particle velocity. Through a modeling simulation, it has been shown that WC-CoCr particles are fully molten during HVOF spraying when their size is smaller than 15 μm [13,17]. Several studies have been performed to investigate mechanical properties and tribological performance of HVAF WC-based coatings [10–12,18–21], among which a few have investigated influence of particle size [20,21]. Bolelli et al. [21] studied sliding and abrasive wear performance of HVAF-sprayed WC-CoCr with two different particle size ranges of 5–30 μm and 15–45 μm employing M3 and M2 guns (Uniquecoat Technologies LLC, USA). Their results showed that coatings deposited from powders with finer particle size yield superior wear performance. The main objective of this study was to compare the tribological properties of HVOF and HVAF WC–10Co4Cr coatings and this was conducted by employing powders of two particle sizes without considering influence of nozzle configuration. Matikainen et al. [20] deposited two different powders with particle size ranges of 10–30 and 5–25 μm using an identical HVAF M3 gun configuration. Average measured temperature of in-flight particles was 50 °C higher for coarser cut size (1410 °C vs. 1360 °C) while the particle velocity for the finer powder was around 30 m·s^{-1} higher than that for the coarser powder (957 m·s^{-1} vs. 929 m·s^{-1}). Average Vickers hardness was slightly higher for coatings sprayed with the coarser powder, with a value of 1458 HV0.3 as compared to 1344 HV0.3 for coatings sprayed with a finer cut size. The main focus of this effort was to evaluate cavitation, slurry and dry particle erosion of WC-10Co4Cr and Cr3C2-25NiCr coatings sprayed by HVOF and HVAF and two different size ranges for the powders were used without considering influence of nozzle configuration.

Table 1
Specifications of the three powders with different particle size used in the study.

Code	Chemistry	Particle nominal size (μm)	Particle size distribution (μm)			Type	Trade name
			D 10%	D 50%	D 90%		
Pc	WC-Co-Cr 86-10-4	45/15	22	34	52	Agl. & Sint.	Amperit® 558.074
Pm	WC-Co-Cr 86-10-4	30/5	12	19	28	Agl. & Sint.	Amperit® 558.059
Pf	WC-Co-Cr 86-10-4	20/5	6	13	22	Agl. & Sint.	Amperit® 558.052

Different nozzle configurations can potentially affect the quality of deposited coating and need to be properly selected based on particle size used as feedstock. The studies mentioned above indicate that selection of an appropriate feedstock particle with a suitable nozzle configuration could result in an enhanced wear performance. Notwithstanding the above, none of the existing studies have undertaken a dedicated effort focused on investigating the effects of particle size and nozzle configuration when spraying WC-based coatings using HVAF. Hence, conducting a comprehensive study, involving a wide range of particle size distributions and a host of different nozzle configurations, to assess how each can influence microstructural, mechanical and tribological properties of HVAF sprayed WC-CoCr coatings is deemed crucial and provides the motivation for this work. Accordingly, a comprehensive investigation is conducted on three powders with different particle size ranges sprayed with four different nozzles with varying length and/or convergent-divergent design to investigate the influence of nozzle configuration and particle size on characteristics and sliding wear performance of HVAF-sprayed WC-CoCr coatings.

2. Experiment procedure

2.1. Spraying process

Three commercially available WC-10Co4Cr powders with different particle size ranges produced by Höganäs GmbH employing the agglomeration and sintering technique (see Table 1), were used as feedstock material. Domex 355 coupons of diameter 25 mm and thickness 6 mm were used as substrates.

An M3 HVAF torch (Uniquecoat Technologies LLC, Oilville, VA, USA) was used and four different De Laval nozzles (Fig. 1) were employed to spray the feedstock powders. All three powders were sprayed with each nozzle configuration in this study, except Pf which was not sprayed with nozzle N3.

Cleaned samples were mounted on a rotating fixture and grit-blasted employing alumina powder. Then the three powders were sprayed with the process parameters mentioned in Table 2 with a targeted thickness of 250 μm for all the coatings. The carrier gas was Nitrogen. It is relevant to

Table 2
HVAF spraying parameters used for coating deposition.

	Pc				Pm				Pf			
	N1	N2	N3	N4	N1	N2	N3	N4	N1	N2	N3	N4
Air (psi)	111	114	113	114	111	114	118	118	111	114	–	118
Fuel 1 (psi)	100	100	105	105	100	100	105	105	100	100	–	105
Fuel 2 (psi)	105	105	115	115	105	105	115	115	105	105	–	115
Carrier ($l{\cdot}min^{-1}$)	40	40	50	50	50	50	50	50	50	50	–	50
Feed ($g{\cdot}min^{-1}$)	200				200				200			
SoD (mm)	300				300				300			
Number of strokes	11	13	11	11	15	17	16	17	26	29	–	26

mention that the HVAF torch technology is critically based on the orifice design inside the torch. Moreover, the fuel and air supply are pressure controlled, not flow controlled. Therefore, an appropriate way to describe torch parameters in a M3 MVAF torch would be to indicate the nozzle dimensions (as done in Fig. 1) and the supply pressures for Air, Fuel 1 and Fuel 2 (provided in Table 2). Nonetheless, it may be added for completeness that, the air and fuel pressures stated in Table 2 for nozzle dimensions indicated in Fig. 1 correspond to flow rates in the range of 9000 l/min for Air and 200 l/min for Fuel 1 and 2.

AccuraSpray – G3C (Tecnar, Quebec, Canada) was employed to measure temperature and velocity of in-flight particles at impact. In order to assess repeatability of measured data, the measurement was repeated three times for Pf sprayed using N1 and N2 nozzles several days apart.

2.2. Characterization of powders/coatings

Scanning electron microscopy (SEM) analysis was performed on all powders to examine their morphology and cross-sections. Powders were collected on carbon tapes and observed under SEM (HITACHI TM3000 microscope, Krefeld, Germany, and ZEISS GeminiSEM 450, Oberkochen, Germany). In order to perform cross-sectional observations, powders were mixed with epoxy, cold mounted, ground and polished (employing the same procedure explained in next paragraph) before being studied in the SEM.

Employing a surface roughness tester (Surftest 301, Mitutoyo, Japan), roughness values of as-deposited coatings (R_a) were measured as per ASME B46.1 standard. Three measurements were performed on each coating and average values and standard deviations have been reported herein.

After sectioning and hot mounting, the samples were ground and polished. Grinding was performed by employing a 45 μm diamond disk, while polishing was carried out successively using 9 μm and 3 μm Kemet liquid diamond solution. Finally, the specimens were mirror-polished employing MasterMet 2 dispense. General microstructure analysis of the samples was performed using SEM analysis.

Vickers hardness of the samples was measured employing Struers Duramin-40 microhardness tester (Cleveland, United States). Fifteen indentations were performed on each sample according to the standard ASTM E384 [22].

Identification of the crystalline phases was performed by X-ray diffraction analysis (XRD), with a Philips X'Pert device (PANalytical B. V., The Netherlands) on as-coated surfaces. XRD measurements were carried out at 40 kV and 40 mA, with Cu Kα radiation (λKα1 = 1.540598 Å, λKα2 = 1.544426 Å), with a scan range of 20°–80° (2θ), step size 0.02°, and an acquisition time of 2 s/step.

2.3. Ball-on-disk test

Sliding wear tests were performed on samples with a mirror-polished surface (ground and polished in the same manner as described in the Section 2.2), following the procedure prescribed in ASTM G99 standard [23]. The test was conducted using a tribometer rig (Tribometer TRB^3, Anton-Paar, Switzerland) which monitors friction coefficient during the test. Alumina balls with radius of 6 mm were employed as the mating counterpart. The ball-on-disk tests were conducted under a constant normal load of 20 N, with a constant linear speed of 0.2 $m{\cdot}s^{-1}$ and for a total sliding distance of 5000 m. At least two repetitions were performed for each test on radius 7 and 9 mm of wear trace. All the tests were done at room temperature with relative humidity of around 30%. After each test, wear products were collected from the surface of the sample in the form of debris, and then the samples were cleaned ultrasonically prior to surface analysis. The top-surface of the wear tracks as well as the wear debris were characterized using SEM/EDX analysis.

Volume loss in the samples as a result of sliding wear was measured employing white light interferometry (WLI) technique (Profilm 3D, Filmetrics, Unterhaching, Germany). Using WLI, it was not possible to capture the whole wear track. Therefore, volume loss in four different regions across the wear track was measured (Fig. 2(a)), based on which an average cross-sectional area was obtained for the wear track at once. Hence, four different wear track locations, approximately 90 degrees apart were scanned on each circular wear track. The overall volume loss was calculated by multiplying the average cross-sectional area by the total length of the wear track (Eq. (1)). Also, specific wear rate for balls

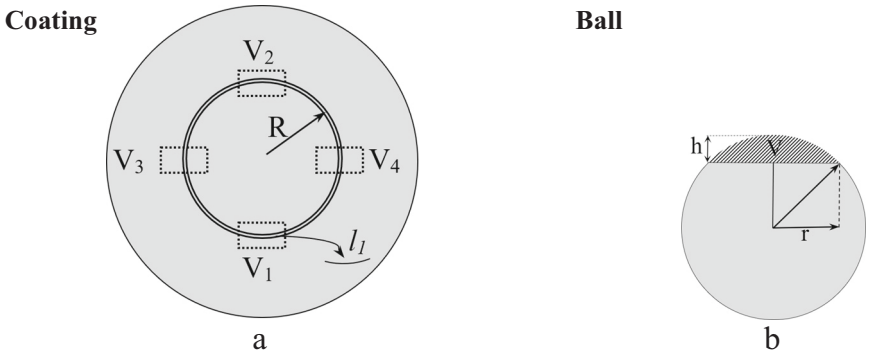

Fig. 2. Schematic sketch of volume loss measurements on a) wear track on coating and b) worn ball.

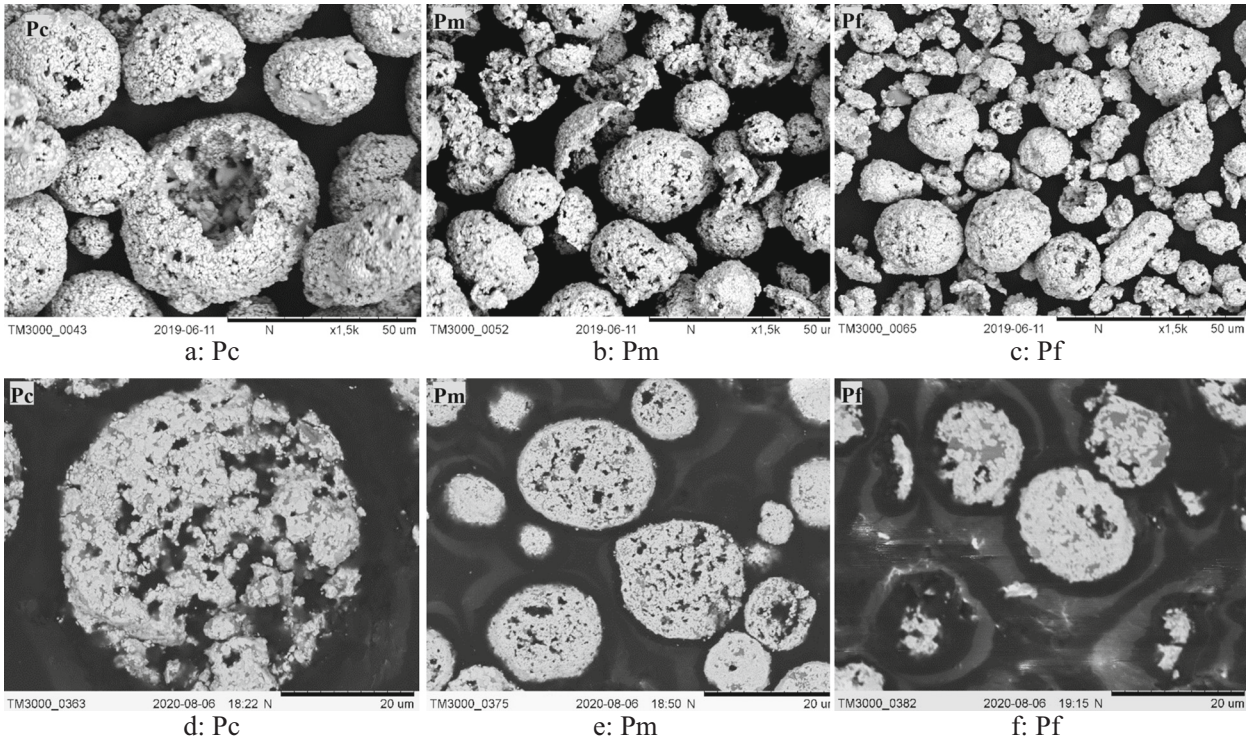

Fig. 3. SEM images of (a-c) particle surface morphologies and (d-f) particle cross-sections of the three powders used (coarse: Pc, medium: Pm and fine: Pf).

corresponding to wear track radius of 7 mm was measured. For this, the worn surface area of balls (see Fig. 16) was measured using image analysis [24], then the corresponding radius (r) and volume loss determined as shown in Fig. 2(b). Consequently, using Eq. (3), the specific wear rates for both the ball and the coating were obtained by dividing volume loss over the normal load (L) and sliding distance.

$$V_{loss-coating} = \frac{1}{2}(\pi.R)\left(\frac{V_1}{l_1}+\frac{V_2}{l_2}+\frac{V_3}{l_3}+\frac{V_4}{l_4}\right) \quad (1)$$

$$V_{loss-ball} = \frac{1}{6}(\pi.h)\left(3.r^2+h^2\right) \quad (2)$$

$$W = \frac{V}{L.d} \quad (3)$$

where in Eq. (1) V_{1-4} are volume losses at the four scanned locations, l_{1-4} are the lengths of the corresponding wear track segments at these locations and R is radius of the wear track. In Eq. (2), h and r are the height and radius of the removed spherical cap, respectively. Finally, in Eq. (3), W is specific wear rate, V is volume loss, L is load and d is total sliding distance.

3. Results

3.1. Powder characteristics

Morphologies of the three used powders are shown in Fig. 3(a), (b) and (c). Most of the powder particles of Pc and Pm exhibit a spherical shape while most of the Pf particles were irregular in shape. Fig. 3(d), (e) and (f) shows cross-sectional images of Pc, Pm and Pf, respectively. From the SEM visualization, it is clear that by decreasing the particle size, the number and dimension of the pores within the particles decreases because the smaller the dimension the limited number and size of comprising defects [25]. In other words, the density of individual particles seemed to increase with decrease in particle size, which can potentially have an influence on density of the resultant coating.

3.2. Deposition rate

Fig. 4 shows the measured in-flight temperatures and velocities of particles, in case of different powders used and nozzle configurations employed. Indicative standard deviation values are drawn as error bars in the corresponding data points, based on repeat measurements

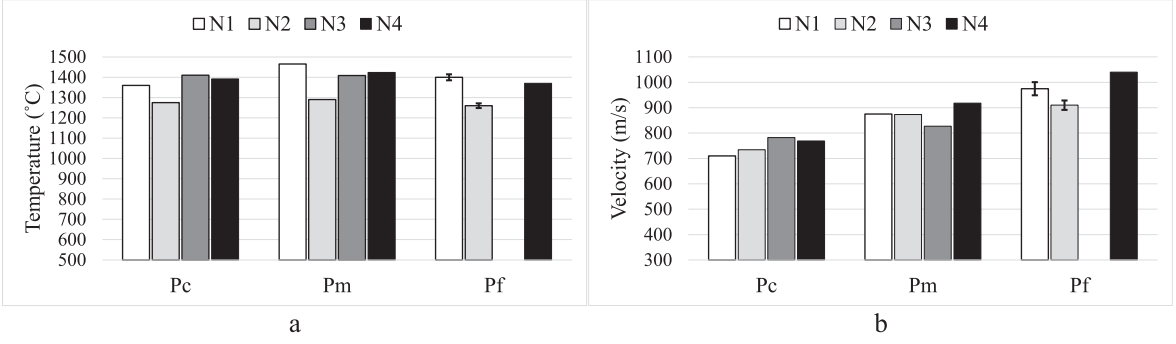

Fig. 4. Measured in-flight a) temperature and b) velocity, for the three feedstock powders sprayed using four different nozzles.

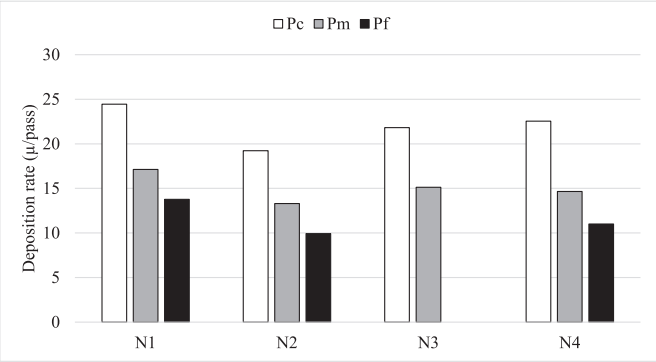

Fig. 5. Deposition rate for various feedstock powders sprayed using four different nozzles.

conducted on Pf sprayed using nozzles N1 and N2 to show reliability of data. The particle temperature was not significantly influenced by the particle size, varying over a window of 105 °C or less when using the same nozzle. Increasing the exit diameter of the nozzle from N1 to N2, led to a drop in particle temperature by around 150 °C for Pf and Pm and by about 100 °C for Pc. The particle velocity was found to increase with reducing particle size in case of each of the nozzles. However, for a given powder, no significant differences in particle velocity were discernible with change in type of nozzle, with the noted variation being limited to a maximum of around 100 $m \cdot s^{-1}$.

An average targeted thickness of around 250 μm was achieved for all the coatings. From the measured coating thickness and the total number of strokes for each coating (see Table 2), the thickness built up per pass (deposition rate) can be determined, which is a fair measure of deposition efficiency. The deposition rates for all the coatings are provided in Fig. 5.

In general, a substantial decrease in deposition rate can be observed with decrease in particle size from Pc to Pm and from Pm to Pf. This trend was consistent and more clearly evident when comparing the deposition rates for each nozzle used for spraying the three powders with varying particle size ranges. The reason for this must be related to the intrinsic properties of particles associated to their dimension and is further discussed in Section 4.1.

Reduction in deposition efficiency may raise concerns around costs. However, it is worth mentioning that deposition efficiency is not the only determining factor governing the choice of feedstock. For example, a finer feedstock particle size makes it possible to fabricate thinner coatings which involve less powder being used in a shorter spraying time and can, in turn, reduce total coating costs. Also, a finer particle size makes it possible to achieve smoother coatings, which can potentially reduce the demand for subsequent machining leading to significant savings in post-processing costs. On the other hand, in this study, powders of all particle sizes were sprayed with a fixed set of parameters. Therefore, the "optimum" spray conditions in terms of deposition efficiency, which could vary with particle size, may not have been encompassed in the process parameter window that has been investigated herein in case of all powders.

3.3. Coating microstructure

Fig. 6 shows SEM images of surfaces of the Pc, Pm and Pf coatings sprayed with the nozzle N2. It is clearly noticeable that, with decrease in particle size, the surface of the coatings attains a finer morphology, resulting in a lower average roughness. Average *Ra* value decreases from around 4.5 μm for Pc coating to around 2.5 μm and 2 μm for Pm and Pf, respectively. No significant difference was observed in surface morphology and roughness of the coatings of the same particle size sprayed with different nozzles.

Fig. 7 shows SEM images of all the eleven coatings. No significant differences in microstructure were detected by changing the nozzle configuration for the same powder. However, with decrease in particle size, the homogeneity of the coatings seemed to experience a substantial improvement. The number and size of the dark regions, which correspond to either pores or binder accumulation (see Fig. 17), considerably decrease with reduced feedstock particle size. In order to differentiate pores, SE SEM images were taken from the polished surfaces of coatings from the three different powders (Fig. 8). It was clear that the size and number of pores dramatically reduced with decrease in particle size from Pc to Pm or Pf. The Pf coating exhibited the highest density among all, with minimal detectable pores observable in the coating at 5000× magnification (shown by arrows). There could be two main reasons for this: first, as discussed before, porosity within the particles decreases with size and consequently yields a denser coating. Besides, as shown in Table 2, the number of passes needed to reach the targeted thickness substantially increased with decrease in feedstock particle size despite the same powder feed rate, which leads to a greater peening effect [26]. This effect can be even more pronounced considering the higher in-flight particle velocity for smaller cut size powders (see Fig. 4), and consequently result in an improvement in the final density of the corresponding coating.

3.4. X-ray analysis

Since all powders were of identical chemistry, X-ray diffraction analysis was performed on one of the powders (Pc) as well as two of the coatings deposited using the coarsest and the finest powders (Pc and Pf) employing N1 and N4 nozzles. As shown in Fig. 9, no deviation in phase constitution is recognizable when comparing all the coatings with the starting powder. This implies that negligible decarburization or phase change occurs when spraying WC-CoCr feedstock powder through HVAF within the process parameter window used in this study. This reaffirms findings from other studies employing the HVAF technique [27].

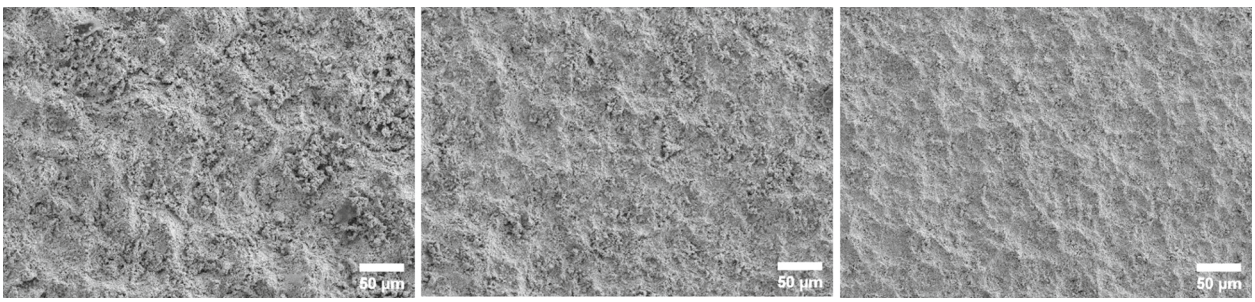

Fig. 6. SE SEM images of surfaces of as-deposited coatings using powders with three different particle sizes (Pc, Pm and Pf) sprayed with the same nozzle (N2).

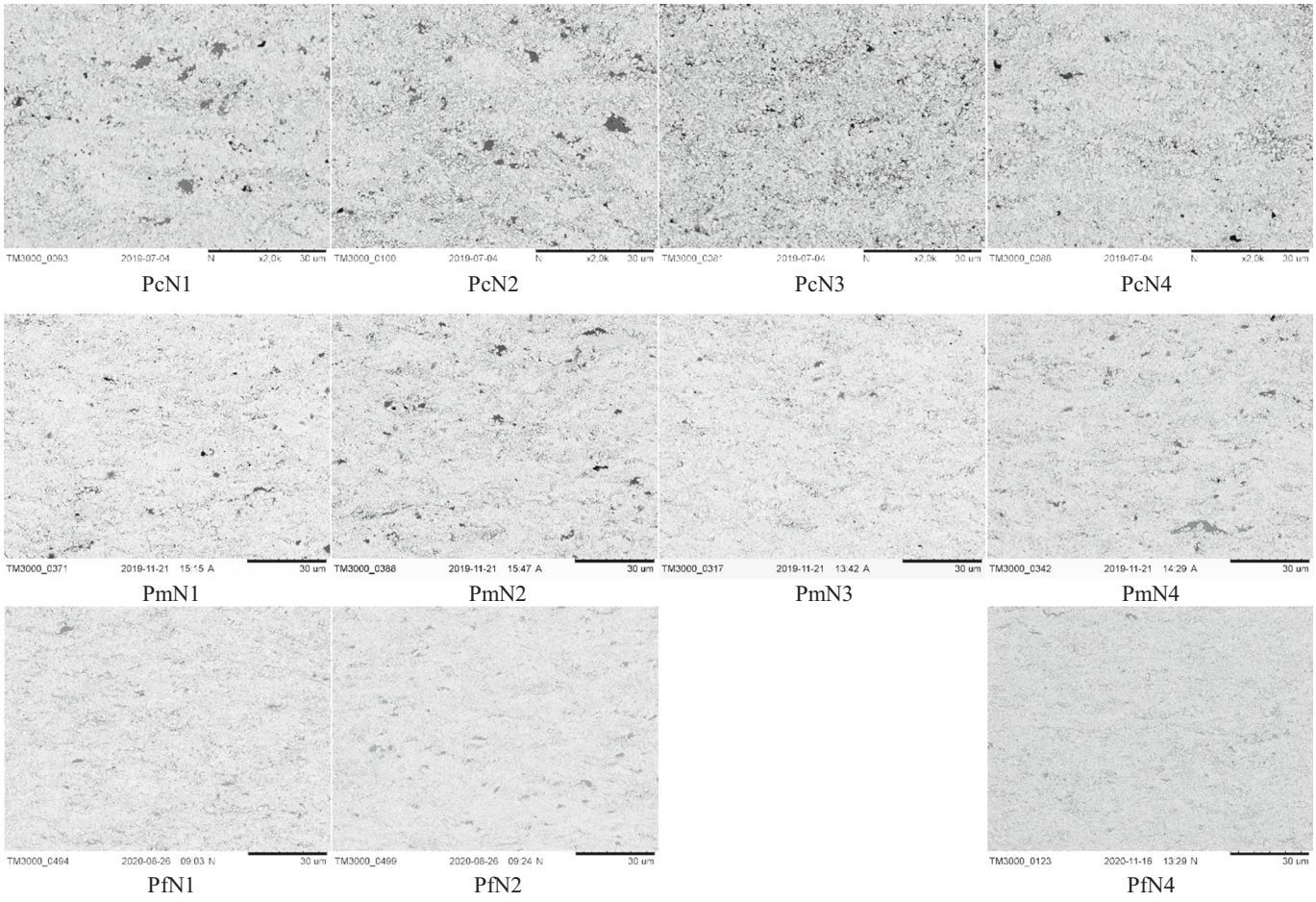

Fig. 7. Cross-sectional BSE-SEM images of all the coatings using powders with three different particle sizes (Pc, Pm and Pf) sprayed with four nozzles (N1, N2, N3 and N4).

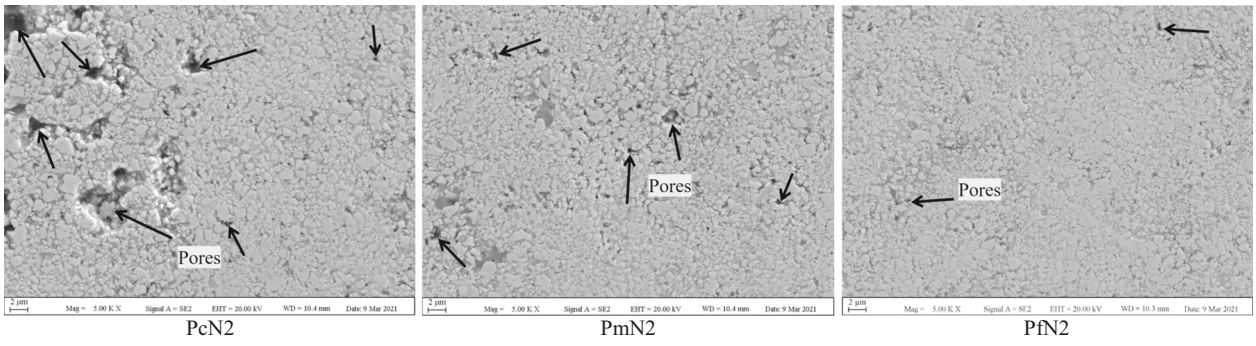

Fig. 8. SE SEM images of surfaces of the three coatings using powders with three different particle sizes (Pc, Pm and Pf), sprayed with the same nozzle (N2).

3.5. Microindentation test

Results from indentation testing show that the Vickers hardness values experience a considerable increase with decrease in particle size, increasing from around 1100–1300 HV0.3 for Pc coatings, to 1350–1450 HV0.3 for Pm coatings, and to 1500–1600 HV0.3 for Pf coatings (see Fig. 10). This is attributable to the denser coatings being formed by decrease in particle size, combined with the stronger peening effect resulting from higher velocity for finer particles as well as the higher number of strokes required due to the lower deposition rate to achieve the targeted thickness [28,29]. Average hardness value of the coatings manufactured from Pc slightly increases with increasing length of the nozzle and/or increasing degree of divergence (larger exit diameter) of the nozzle (N3/N4 vs. N1/N2). The reason for this could be the slight increase in particle velocity as seen in Fig. 4 and the corresponding increase in peening effect. This effect of velocity on peening effect has also been confirmed by other studies [20,25]. For each particle size (Pc, Pm and Pf), average hardness values are highest for coatings sprayed by nozzle N4 as evident from Fig. 10.

3.6. Sliding wear

By calculating specific wear rates of each coating and corresponding mating ball, as well as monitoring coefficient of friction (CoF) values

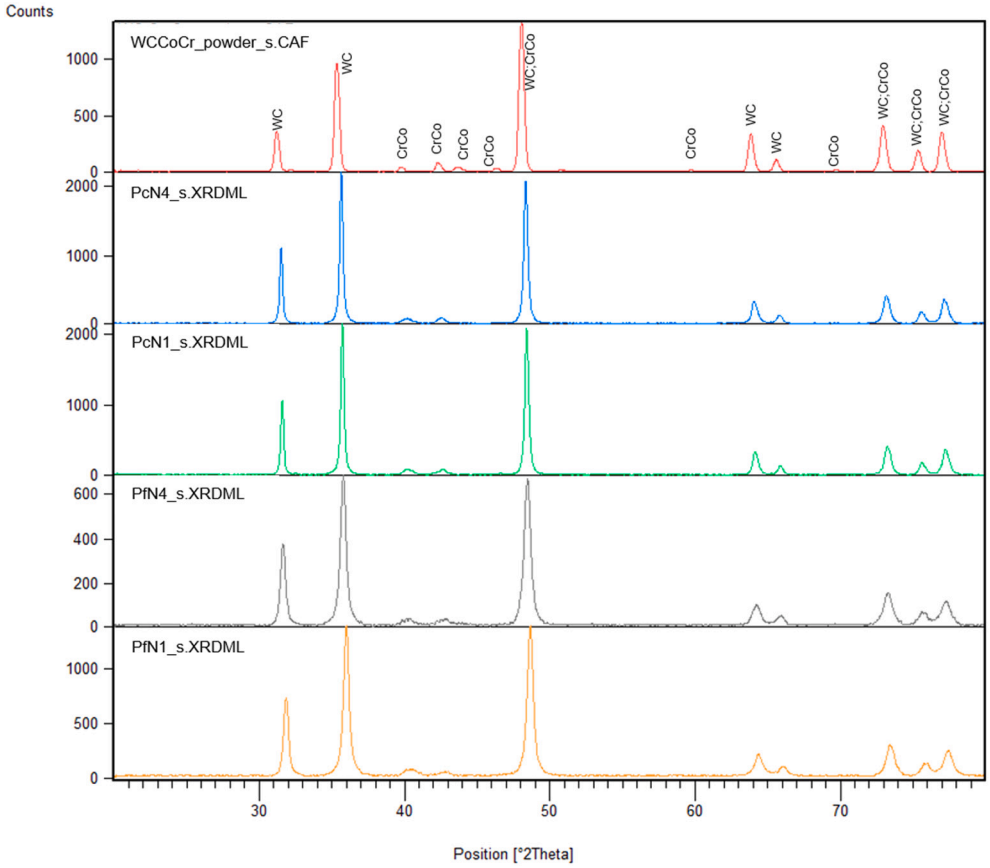

Fig. 9. XRD spectra of the Pc powder along with PcN1, PcN4, PfN1 and PfN4.

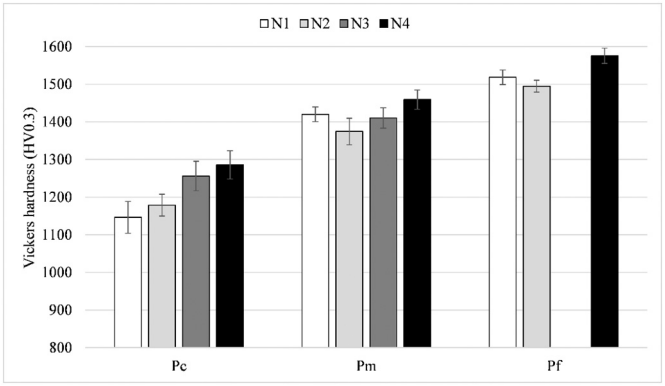

Fig. 10. Vickers microhardness values for all coatings sprayed with various nozzles and powders with different particle size.

throughout the duration of the wear test, an effort was made to compare all the coatings in terms of their sliding wear performance. Also, a comprehensive post wear analysis was performed to shed light on prevailing material removal mechanisms.

Fig. 11(a) shows average values of friction coefficient for all the coatings after the initial running-in period (after 10,000 s). Error bars show standards deviation in the CoF values calculated based on the test repetitions. It can be seen that, with the sole exception PfN2, the average value for all the other coatings decreases with decrease in powder cut size. For Pc and Pm, the average value of friction coefficient was not found to be dependent on the employed nozzle. Pf sprayed by N2, on the other hand, had an average coefficient of friction that was about double as that of PfN1 and PfN4. The reason for this is not clear, but it could be just an outlier value in CoF which is usual to happen in these coatings, as it was shown in our other study [30]. It was also shown in the above study that there was no correlation between the CoF value and the specific wear rate.

In Fig. 11(b), evolution of friction coefficient of the three coatings from Pc, Pm and Pf powders sprayed using nozzle N1 is shown. It can be seen that all the coatings follow the same generic trend, with the CoF attaining a steady state after around 10,000 s. Also, it is clear that the CoF value decreases with decrease in particle size. Notably less fluctuation in CoF values (during steady state period) can be observed for Pf when compared to Pm and Pc, as well as for Pm when compared to Pc. It is discussed later in Section 4.2 that the reason for reduction in CoF value as well as its fluctuation can be related to the initial powder particle size and consequently the size range of the ensuing debris. Coatings fabricated from smaller feedstock particle size led to production of finer wear debris, resulting in lower CoF and less fluctuation.

Fig. 12(a) shows specific wear rates of all the coatings. Specific wear rate was extremely low and of the order of magnitude of 10^{-8} $mm^3 \cdot N^{-1} \cdot m^{-1}$ in all cases. Moving to finer powder cut size from Pc to Pm, regardless of the nozzle type, the average value of specific wear rate of the coatings was found to decrease. Further decreasing particle size (Pm to Pf) leads to further decrease in specific wear rate of the coatings sprayed employing nozzles N2 and N4. The coatings deposited with medium and fine sized powders performed similarly, one of the reasons being that the difference in particle sizes between the two powders was not as large as that between medium and coarse powders (see Table 1). Among all the three powder cut sizes, Pm showed the least sensitivity to the type of nozzle, with the average specific wear rates of all the four coatings deposited with different nozzles being in the narrow range of 14×10^{-8} $mm^3 \cdot N^{-1} \cdot m^{-1}$ to 21×10^{-8} $mm^3 \cdot N^{-1} \cdot m^{-1}$. Pc and Pf sprayed by nozzle N1 exhibited the least resistance against wear while Pf sprayed using nozzle N4 accounted for the best performance among all coatings.

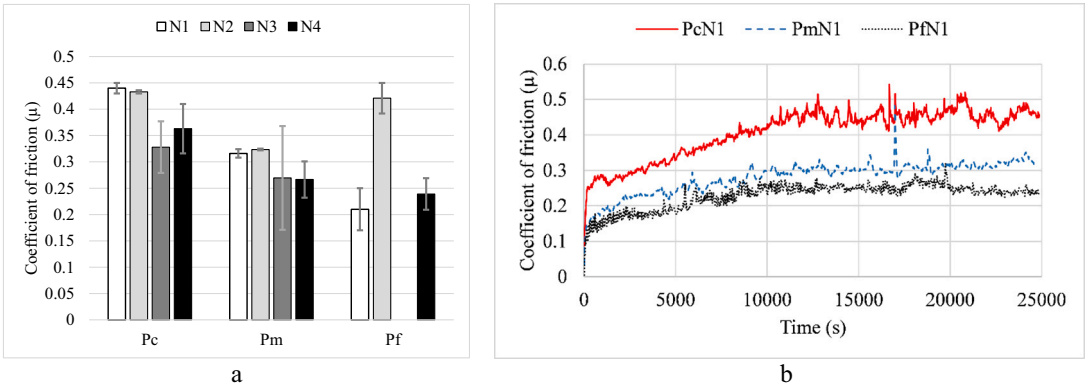

Fig. 11. a) Average steady state CoF values for all coatings, and b) typical evolution of CoF for coatings with different powder cut size.

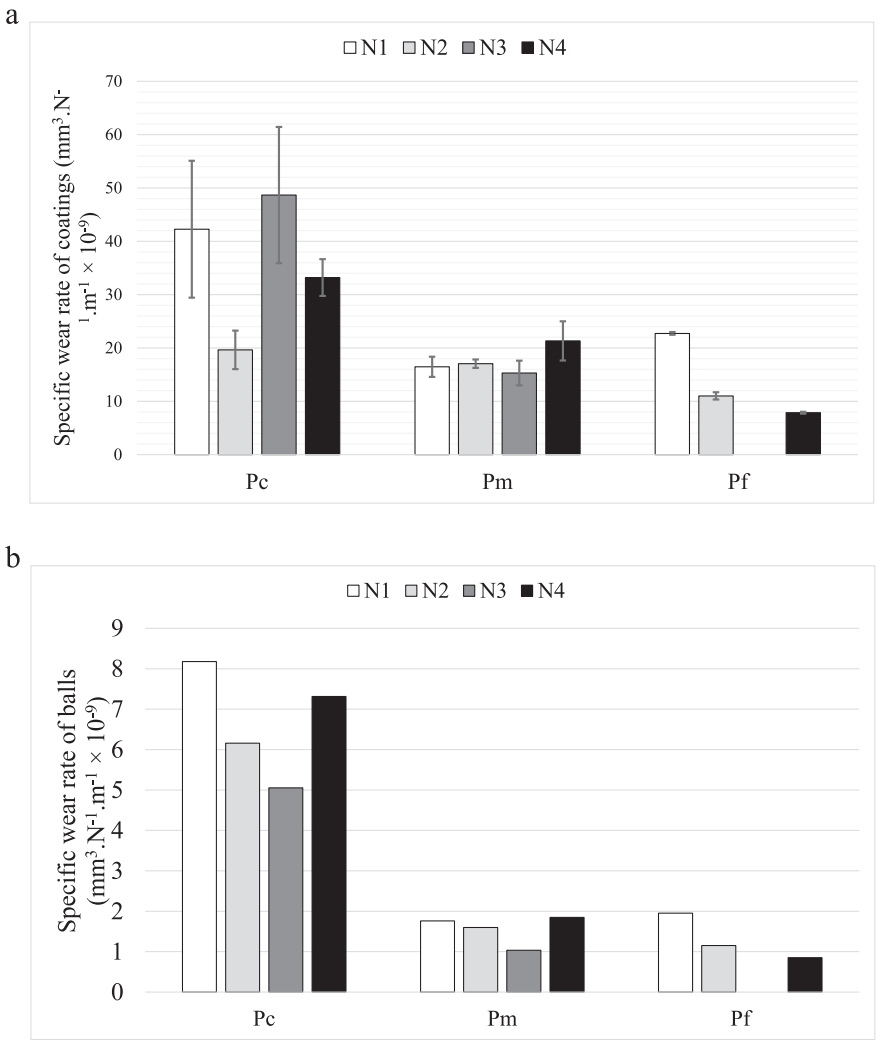

Fig. 12. Specific wear rates of a) coatings, and b) mating alumina balls.

Comparing specific wear rates of the alumina balls used as counter body in each of the wear tests (Fig. 12(b)), it was difficult to establish a clear correlation. However, a general trend can be observed that higher specific wear rate in the coating leads to a higher specific wear rate in the corresponding ball. Powder Pc sprayed with nozzle N3 was the only exception in this regard, showing comparable specific wear rate as PcN1 but the counterpart ball exhibiting much lower wear than that of PcN1 counter body.

Lower specific wear rates and consequently smaller contact surface areas of the corresponding balls (see Fig. 16) in case of coatings fabricated from finer powder cut size, could be correlated with the noted lower coefficient of friction values. This is consistent with other studies reporting that smaller frictional surface can result in lower friction coefficient [31,32].

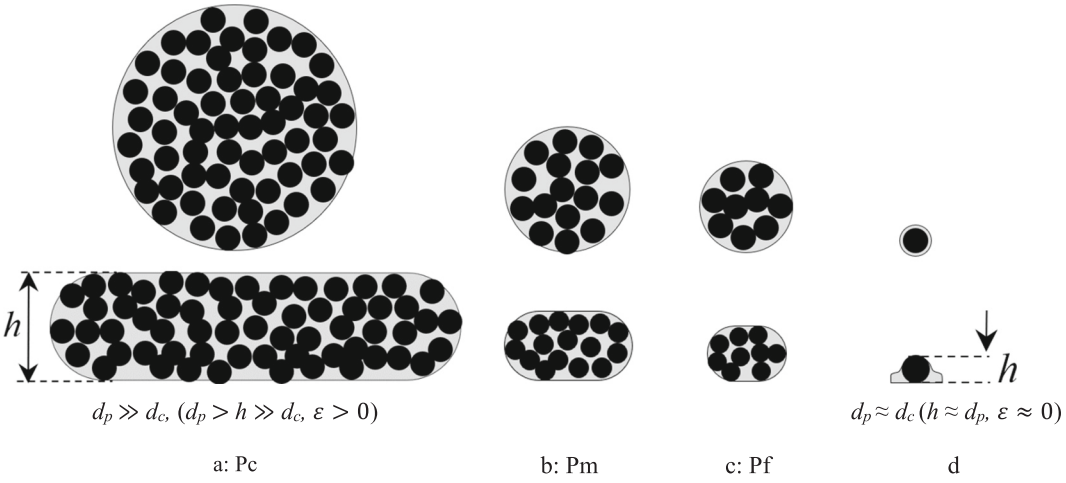

Fig. 13. Schematic illustration of feedstocks Pc, Pm and Pf (a, b and c) and their respective flattening showing the effect of relative powder particle and WC particle sizes on flattening behaviour.

4. Discussion

4.1. Deposition behaviour

The consistent decrease observed in deposition efficiency for each nozzle when particle size is decreased can be discussed from various points of view. According to the literature, it is already known that for WC-based feedstock sprayed by cold spray and HVOF, the size and content of WC particles [33–36], powder porosity [29,37] as well as substrate hardness and roughness [38,39] can all significantly influence the flattening ability of powder particles impacting the substrate and its deposition rate. Presence of an intimate conformal contact surface occurring as a result of particle flattening is essential for good bonding, and can also be beneficial for enhancing deposition efficiency [36,37]. Porous particles show better deformation ability or flattening upon impact compared to dense particles [37] and, as a result, have lesser chance of being rebounded. As discussed in Section 3.1, in case of the feedstocks used in the present study, increase in particle size corresponds to higher porosity content within powder particle and as a result improves flattening ability. This is in line with the studies conducted by Gao et al. [37] on cold-sprayed WC-Co coatings, Varis et al. [29] on HVOF-sprayed WC-CoCr coatings and Chivavibul et al. [40] on warm-sprayed WC-Co coatings. So, better deformability can be one of the reasons for higher deposition rates noted when powder particle size is increased (Fig. 5).

However, besides the porosity effect, the size of particles is another key factor determining flattening behaviour. For homogeneous particles, it has already been shown by experiment and modeling that smaller particles tend to exhibit greater resistance against deformation upon impact [41]. Several studies have been conducted with the aim of understanding the effect of carbide dimensions on flattening behaviour of WC-based coatings [33–35,42]. If the particle is assumed to be spherical, the flattening ratio can be defined as [41,43];

$$\varepsilon = 1 - \frac{h}{d_p} \tag{4}$$

where d_p and h are particle size and the height of flattened particle, respectively.

Depending on the relative size of powder particle (d_p) and carbide particle (d_c), the flattening behaviour can be categorized as follows:

Case I:

$$\delta = \frac{d_p}{d_c} \gg 1, \varepsilon > 0 \tag{5}$$

Case II:

$$\delta = \frac{d_p}{d_c} \approx 1, \varepsilon \approx 0 \tag{6}$$

For Case I, where the particle size is much larger than the carbide size ($\delta \gg 1$), flattening ratio increases with the ratio d_p/d_c and can be calculated theoretically [44]. In this case, the deformability of the particle is governed by equivalent properties of both binder and carbide particles. However, with decrease in size of powder particle (d_p) when the carbide size is constant (d_c), the flattening ratio progressively decreases to the point where the powder particle theoretically comprises only one carbide particle (Case II) and the flattening ratio approaches zero. As the ratio dp/dc approaches 1, solid carbide particles dominate the flattening behaviour. Hence, because of low flattening ratio, the chance of the particle being rebounded off increases. This trend is observed when reducing particle size from Pc to Pm and Pf (Fig. 13(a, b and c)), with decrease in particle size resulting in decrease in δ value and consequently a decrease in flattening ratio (ε) of the particles. This can explain how more particles tend to bounce off and result in lower deposition rate for powders with smaller particles, when carbide size is the same. High chance of particles corresponding to smaller δ values being bounced off after impacting the surface is consistent with other studies [33,42].

Surface roughness is another factor influencing flattening behaviour of particles and, as a result, the deposition rate [45]. It was shown in Section 3.3, Fig. 6, that the three coatings Pc, Pm and Pf are characterized by different progressively decreasing surface roughness values. During spraying, every deposited layer can be considered as the 'substrate' for the next pass. Higher roughness can result in higher induced shear stress on the particle upon impact, which leads to better flattening and, consequently, improved deposition rate [38,45].

According to Accuraspray data (see Fig. 4), decrease in particle size leads to a substantial increase in particles velocity. This can be another key parameter influencing deposition behaviour of powders with varying particle size. In case of cold spray, it has been reported that there exists a critical velocity which the particles must overcome in order to get deposited successfully onto a substrate [46,47]. Similarly, there have also been studies on metallic powders which reveal that, for velocities beyond a certain value, no major difference is noted in deposition efficiency [48,49]. In some cases, it has indeed been shown that increase in velocity can lead to increase in rebounding of particles [35]. Therefore, increase in velocity of powder feedstock containing hard WC particles may not improve deposition rate.

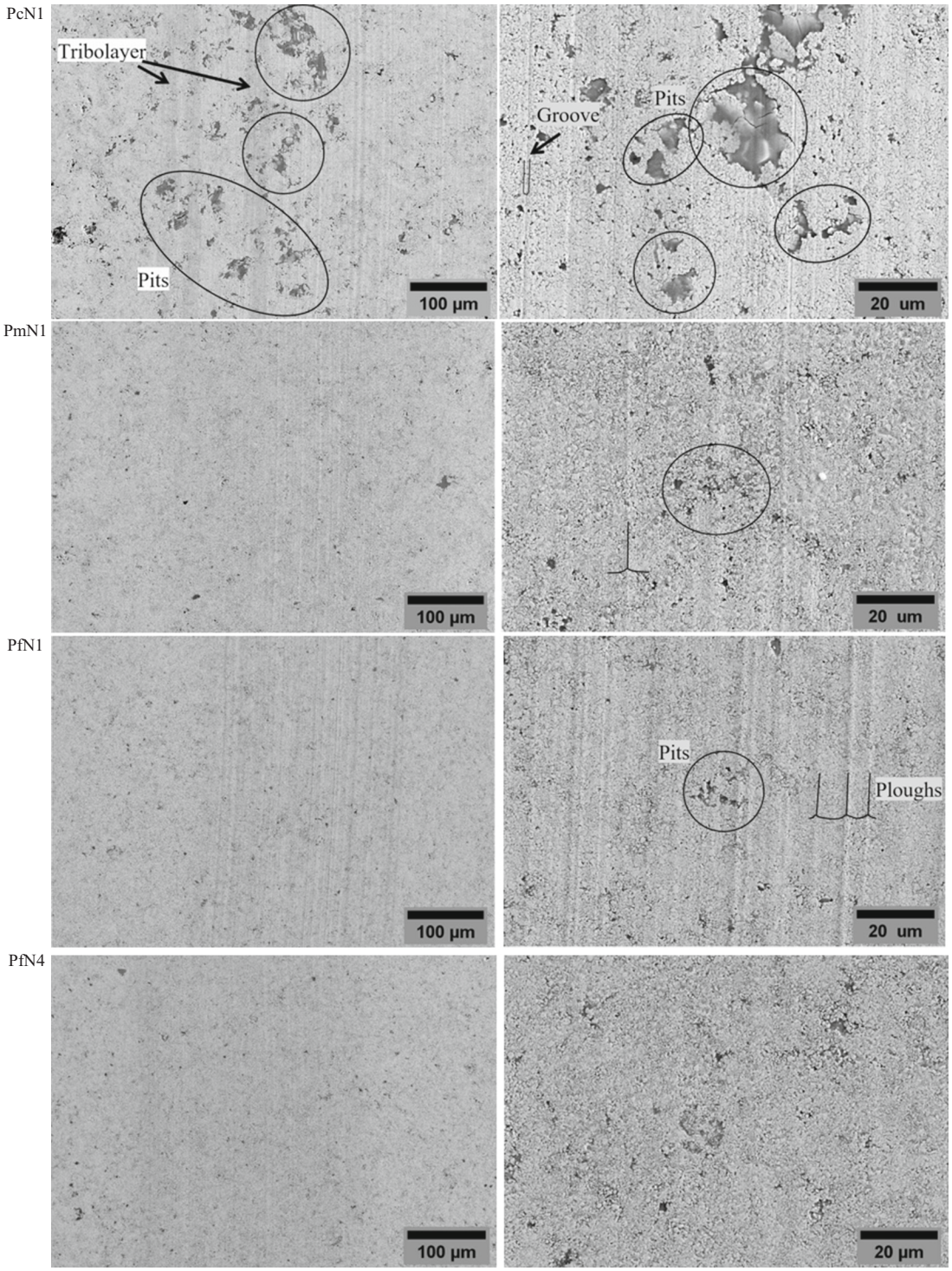

Fig. 14. SE SEM images of wear tracks on the four tested coatings, revealing changes in wear mechanisms with decreasing feedstock particle size. Pit areas are indicated by ellipses/circles.

4.2. Wear behaviour

Fig. 14 shows low and high magnification SEM images taken on wear tracks with the same track radii ($r = 7$ mm) on tested coating specimens fabricated from the three feedstocks Pc, Pm and Pf, sprayed with nozzle N1. Comparing the low magnification images with specific wear rate values (Fig. 12(a)), it can be inferred that samples with deeper and higher number of grooves account for higher specific wear rate values. Another clear difference between the three images is the presence of pits within the wear track of the sample PcN1, which are negligible in the other two samples. These pits could have been formed as a result of breakage of group of carbides resulting in massive exfoliation. It is plausible that the segregated carbides get stuck between sliding ball and sample surface leading to chipping of coating and consequently formation of narrow deep grooves. The other two samples do not exhibit presence of such grooves, and wide shallow ploughing tracks are detectable instead. The tracks are deeper and higher in number for the sample PfN1 compared to sample PmN1. The ploughing tracks could

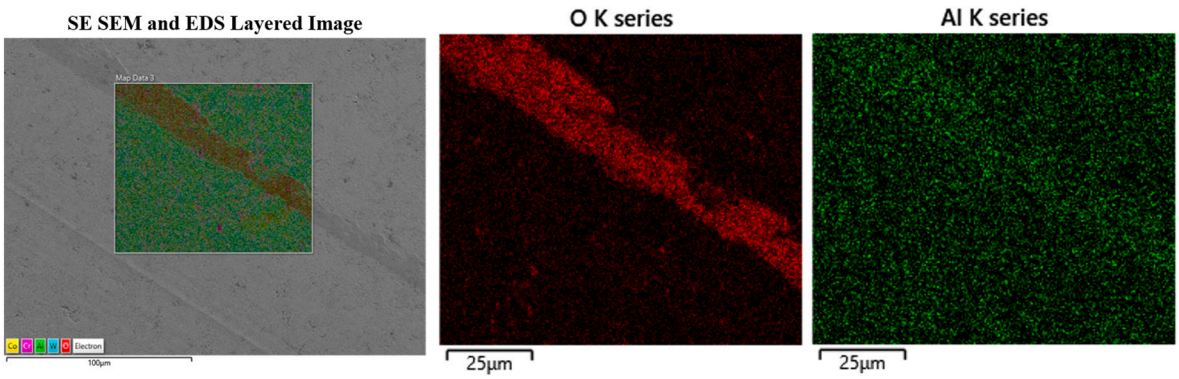

Fig. 15. SE SEM image of tribolayer within the wear track of sample CfN1 along with the layered EDS image on tribolayer and EDS maps of O and Al.

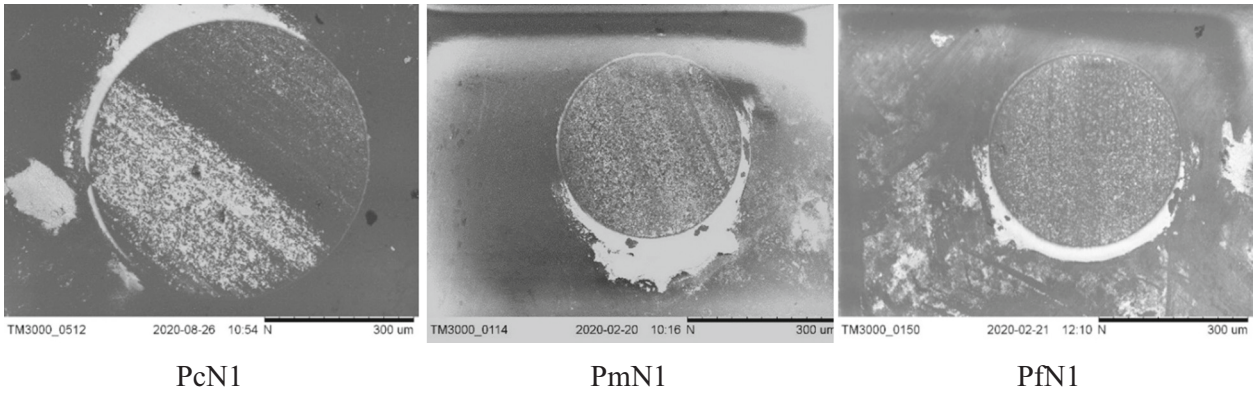

Fig. 16. Wear scars on alumina ball counterbody in case of the three coatings PcN1, PmN1 and PfN1.

have formed as a result of the alumina ball sliding over the surface leading to coating material being pushed aside as well as beneath [50,51]. Using nozzle N4 for spraying Pf resulted in the best sliding wear performance among all the eleven samples. From SEM images of its wear track (Fig. 14), extremely shallow ploughing tracks are detectable without any sign of grooving and carbide fragmentation.

One feature that was observed in some of the wear tracks (e.g. PcN1 in Fig. 14) was the formation of a thin, narrow and smooth tribolayer similar to that reported in a previous study [52]. In some cases, the tribolayer seemed to be thicker and could be distinguished as a distinct layer which is perfectly bonded to the surface. Fig. 15 shows a typical tribolayer within the wear track of sample CfN1. The EDS analysis on the tribolayer reveals presence of W, Co, Cr, Al and O elements, with O being the predominant element and W, Co and Cr showing similar patterns. Hence, the formed tribolayer is essentially a mixture of oxidized elements from the coating as well as alumina from the ball counterpart. Formation of such oxide rich layers has been reported by others, and referred to as tribolayer or tribofilm [52–54]. Presence of a tribolayer can effectively separate the coatings surface from the counterpart ball and, therefore, change the governing tribological behaviour of the

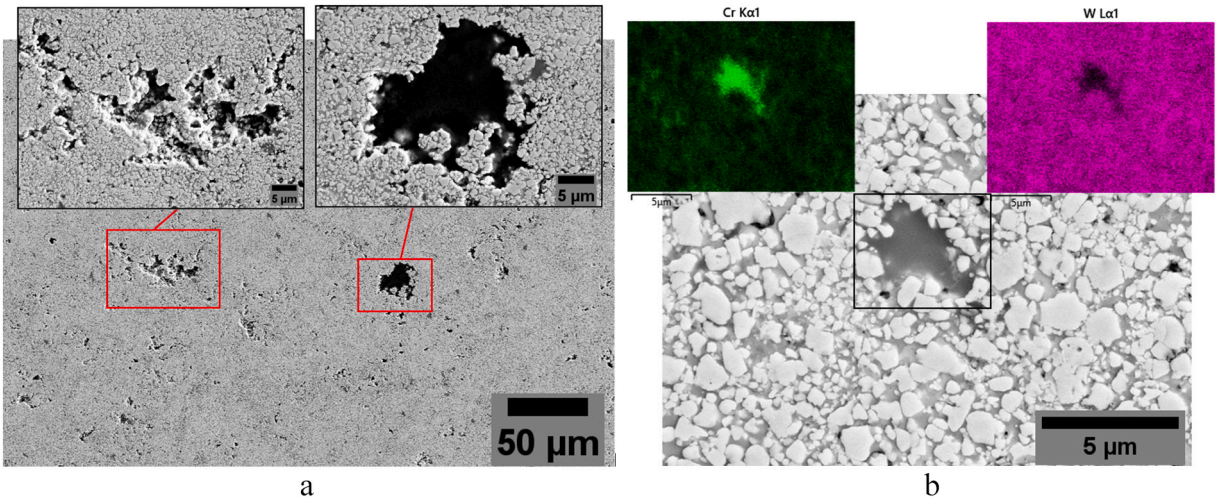

Fig. 17. SE SEM micrographs revealing a) pores and b) binder accumulation region (with corresponding EDS maps) in regions outside of wear track of sample PcN4.

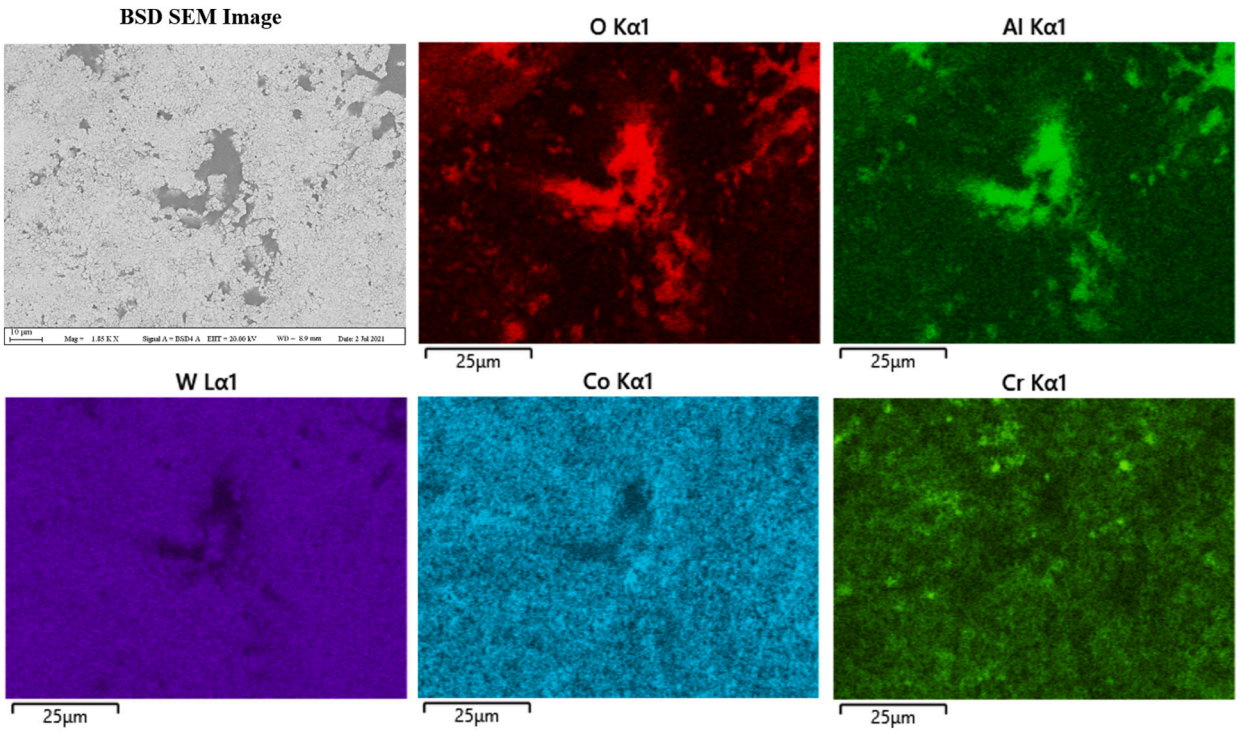

Fig. 18. BSE SEM and EDS micrographs revealing oxide accumulation in pits within wear track of the sample PcN1.

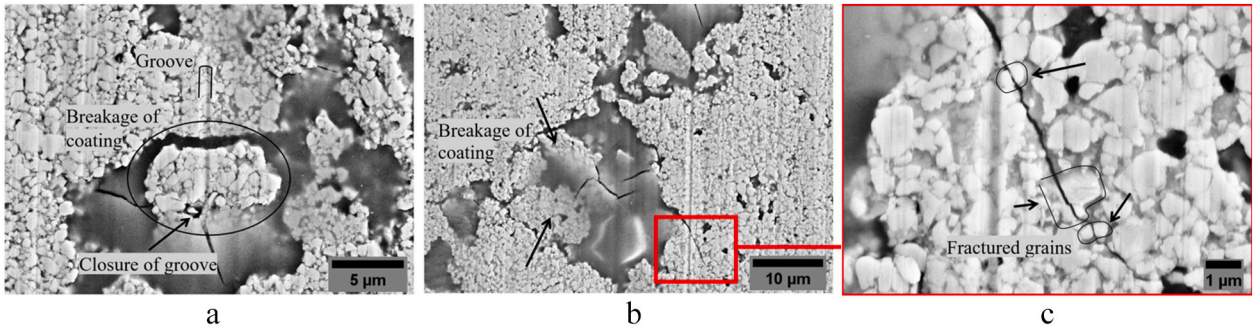

Fig. 19. Breakage mechanism in Pc coatings, a and b) breakage of a fragment of coating, c) intergranular crack initiated from the pit shown in (b).

surface. It has been reported that the presence of such a tribolayer covering the surface of a wear track can significantly decrease the specific wear rate [53–56]. However, the presence or absence of this tribolayer did not seem to significantly influence the specific wear rate or coefficient of friction of the corresponding samples in this study. The reason could be that in none of the samples a continuous and wide tribolayer covering a significant fraction of the wear track could be distinguished.

Fig. 16 shows the wear debris accumulated around the leading edge of the contacting region of the balls. Presence of the wear debris can potentially act as third body particles and facilitate the process of material removal [57,58]. Parallel ploughs on the balls are detectable along the sliding direction and can be attributed to such third body action of particles present in the debris.

It was observed that ploughing was the common mechanism in all the three (Pc, Pm and Pf) coatings. It was also seen that, for coatings fabricated from the coarse powder (Pc), several narrow shallow grooves are visible on the wear track apart from some pits. The presence of these pits was the main identifiable difference between the Pc coatings and the other two (Pm and Pf). These pits could have initiated from small pores and accumulated binder areas (Fig. 17) where there was lack of support for material around the pit. Fig. 17(a) shows high magnification SEM images on shallow and deep pores on the surface of the coating, taken in areas outside of the wear track regions. Fig. 17(b) additionally shows regions of accumulation of binder (in form of pits) outside of the wear track. EDS analysis on the pits shows accumulation of binder rich in Cr in these regions. Similar EDS map was performed for Co and no accumulation of the element was identified. Similar analysis was also performed on pits within the wear track (Fig. 18). It is clear that, unlike the ones outside the wear track (Fig. 17(b)), the pit within the wear track was filled with material transferred during wear testing, which was mostly aluminum oxide from the ball counterbody.

SEM analysis at higher magnifications was performed on the wear tracks to explore breakage mechanism around the pits in more detail. Fig. 19(a) and (b) shows breakage of coating in the form of batches of carbides. In Fig. 19(a), breakage of a fragment was observable and transformed along the sliding direction. It may be pointed out that similar behaviour was observed for coatings with WC-CoCr feedstock of identical chemistry sprayed with another HVAF spray gun (Kermetico, Inc.) [19]. Also, a groove can be detected continuing over the fractured fragment and being closured within the pit (shown by arrow). Existence of the grooves facilitates breakage of fragments because of high amount

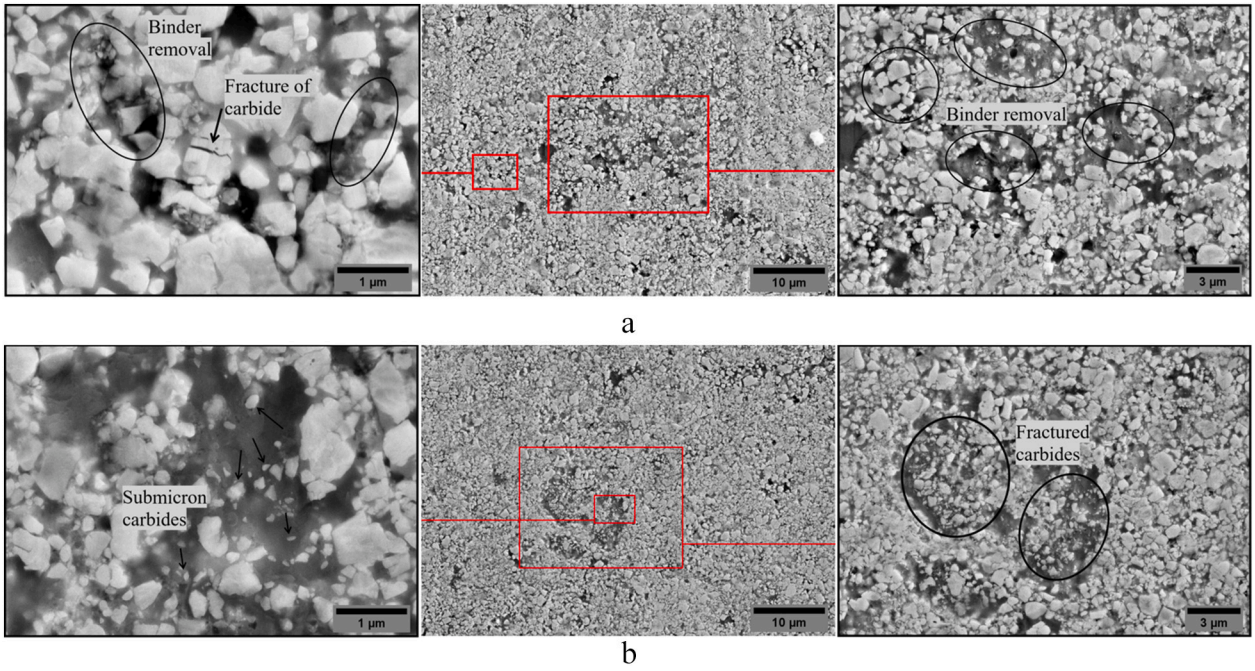

Fig. 20. Breakage mechanisms in coatings a) Pm and b) Pf.

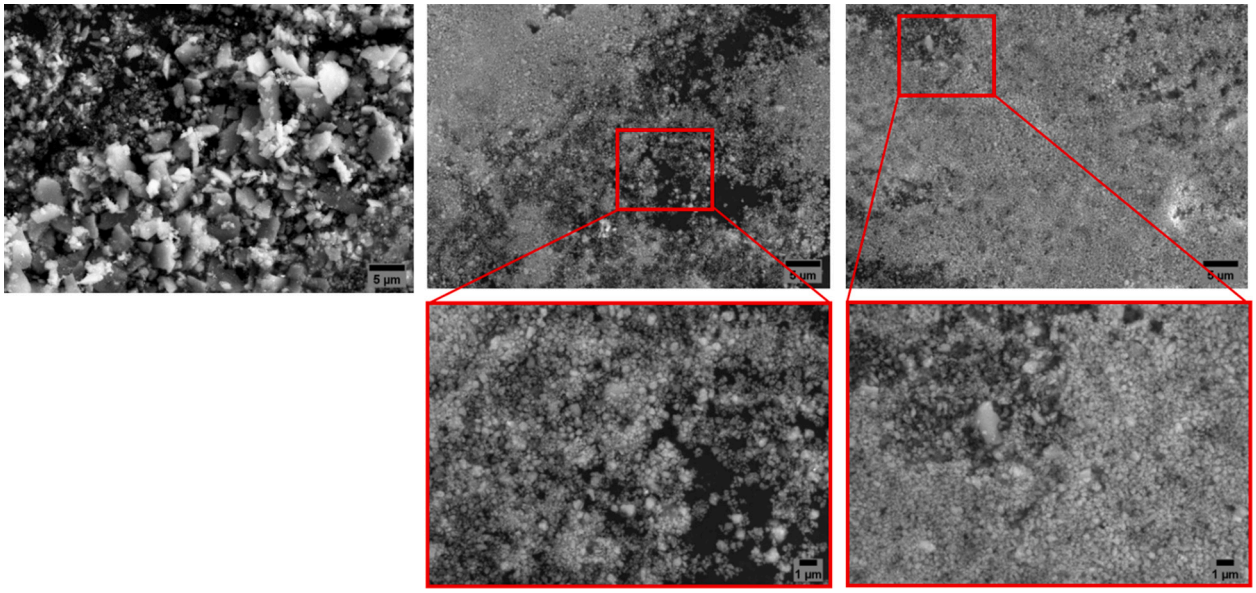

Fig. 21. Wear debris from: a) Pc coating, b) Pm coating and c) Pf coating.

of stressed induced to the coating due to presence of a third body particle. In Fig. 19(b), breakage of several fragments was observable being separated both along the sliding direction and in the opposite direction as shown by arrows. These fragments were possibly fractured in absence of any major third body particle since there was no grooving detectable over these fractured fragments. These pits can introduce some stress concentrated locations leading to crack propagation (shown by the square in Fig. 19(b)) and further breakage into fragments. Fig. 19(c) shows a high magnification image of the crack indicated in Fig. 14(b). It can be seen that an intergranular crack was formed regardless of the carbide's presence towards the next pore. The fractured carbides are identified with red marks.

As discussed, the presence of these pits can facilitate the process of material removal. However, the pits are not reflected as removed material when measuring volume loss, since they are already filled up with wear products. Besides ploughing and grooving as the two common removal mechanisms for Pc coatings, crack initiation and propagation around pits leading to breakage of batches or groups of carbides was the other main wear mechanism. These batches of carbides can be further fragmented into individual carbides as a result of further sliding and removed from the surface. The described mechanisms were similar for the coarse powder sprayed with all the four nozzles (PcN1, PcN2, PcN3 and PcN4). However, in case of Pm and Pf coatings, there was no detectable fragmentation of carbides as a batch.

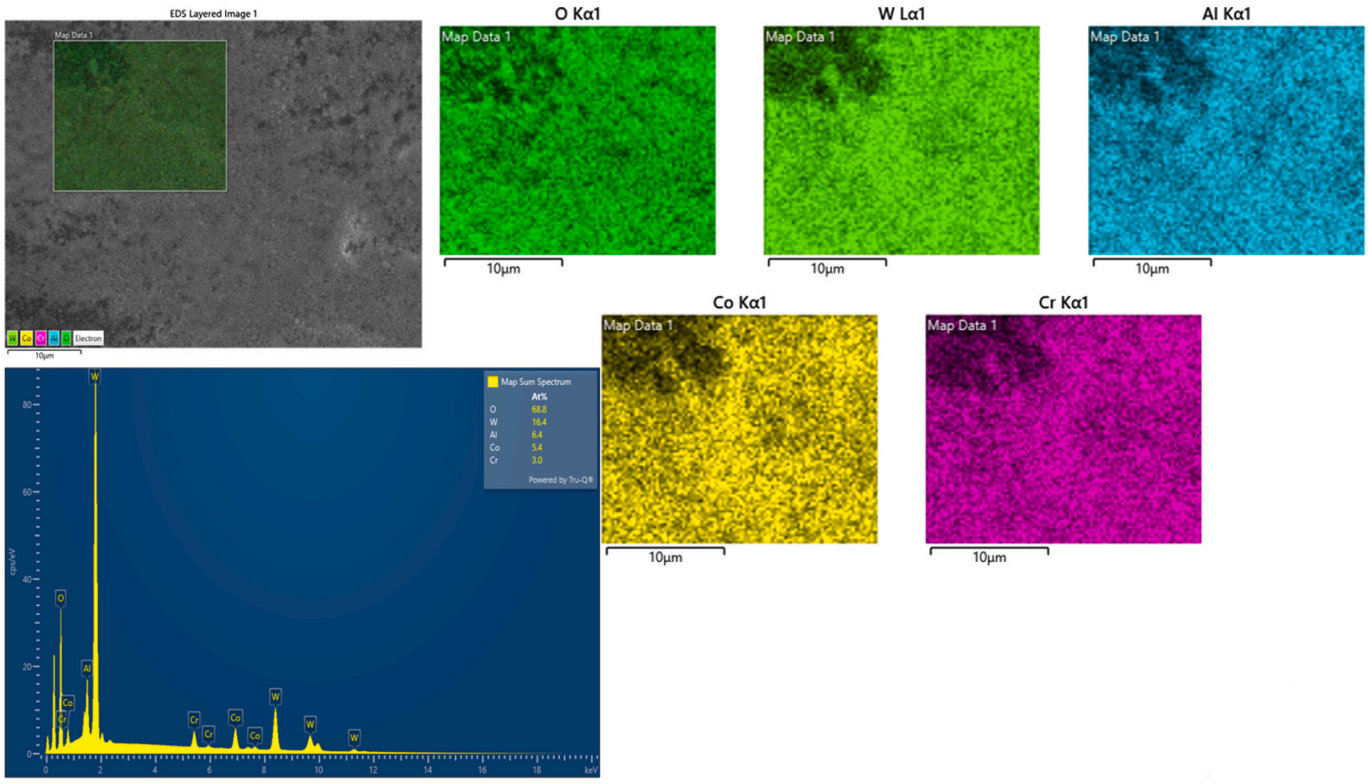

Fig. 22. EDS analysis on wear debris from PcN1 coating.

In both Pm and Pf coatings, there were no signs of pits filled up with wear products. Instead, as shown in Fig. 20, in the first step, binder around carbides seems to be removed resulting in lack of support around the carbides. Then due to load applied from slider, the individual carbides could get fractured, leading to production of submicron sized carbides (shown by arrows in Fig. 20). The last step would be removal of these nano size wear products. SEM investigation of wear debris confirms these differences in wear mechanism between Pc coatings and Pm/Pf coatings.

As shown in Fig. 21, size of debris particles in case of Pc coatings was much coarser and irregular shaped than that observed in Pm and Pf coatings. Fig. 21(a) shows debris produced from Pc coatings, which are mostly in size range of initial carbide particles (1–3 μm). Presence of these micro size carbides acting as third body particles explains higher coefficient of friction during the ball-on-disc tests as shown in Fig. 11. For Pm and Pf coatings (Fig. 21(b) and (c)), very few micro size particles are found in the debris, with a majority of them being in the nanometric size range and spherical in shape.

Comparing dimensions of the wear debris with friction coefficient values (Fig. 11(b)), it is clear that CoF value is reduced with reduction in debris size. For Pm and Pf, the presence of nano-sized spherical shaped debris particles can result in reduction in friction coefficient [31,59,60]. Also, it can be seen that by reduction in debris size, friction coefficient value as well as its fluctuation was reduced.

Semi-quantitative EDS analysis was conducted on debris from PfN1 samples shown in Fig. 22. Elements of O, W, Al, Co and Cr were detectable in debris. The EDS analysis conducted on wear debris from Pm and Pc coatings showed similar result for all.

5. Summary and conclusions

Sliding wear tests were conducted on different HVAF-sprayed WC-CoCr coatings with the aim of evaluating effect of feedstock particle size and spray nozzle configuration on tribological performance of the coatings. Moreover, their influence on coatings' hardness and their microstructural characteristics were assessed by conducting micro indentation test, SEM, EDS and XRD analyses. The main conclusions are listed as following.

- For a given nozzle, reduction in particle size leads to increased density, better homogeneity and higher hardness in the coating. At the same time, the reduction in particle size is accompanied by a reduction in deposition efficiency. Despite the decrease in particle size, negligible decarburization was detected in all the coatings. All these result in better wear performance of the coatings by decreasing the feedstock particle size.
- Fine feedstock powder sprayed with nozzle 5L4 exhibited the best wear performance among all the coatings. Therefore, nozzle 5L4 is recommended for spraying fine powder. However, the specific wear rates of coatings with the medium sized feedstock were independent of nozzle type.
- Although no major change was observed in microstructure of the coatings deposited from the same feedstock particle size but with different nozzle configurations, the average hardness value increased by increasing length of the nozzle and/or its exit diameter (from 4L4/4L2 to 5L4) for all the three particle sizes.
- While shallow and wide ploughing was found to be the common wear mechanism in all the coatings, decrease in feedstock particle size led to a major change in material removal mechanism in the corresponding coating. Wear mechanism for coarse feedstock coatings involved crack propagation around pores and binder accumulation areas leading to breakage of batches of carbides with binder into the pit areas. Further sliding of the ball possibly caused further fragmentation and removal of these batches of carbides, with the debris acting as third body particles to leave narrow deep grooves on the coating surface. In medium and fine feedstock coatings, no pits were observed. In these two coatings, the wear process seems to start with removal of binder and subsequent fracture and fragmentation of loosely bound individual carbides resulting in removal of fine-sized carbides. SEM analysis of debris particles confirmed this difference,

with debris for coarse feedstock coatings being much coarser as compared to the medium and fine feedstock coating debris.

CRediT authorship contribution statement

Kaveh Torkashvand: Conceptualization, Methodology, Investigation, Data curation, Writing – original draft. **Mohit Gupta:** Conceptualization, Methodology, Supervision, Writing – review & editing. **Stefan Björklund:** Investigation, Conceptualization. **Francesco Marra:** Investigation, Data curation. **Lidia Baiamonte:** Investigation, Data curation. **Shrikant Joshi:** Conceptualization, Methodology, Supervision, Writing – review & editing, Funding acquisition.

Declaration of competing interest

No conflict of interest.

Acknowledgements

The authors would like to thank Owe Mårs and Olivia Danielsson from Höganäs for supporting this study through useful discussions and by providing feedstock powders. Also, financial support of the Knowledge Foundation, Sweden for project HiPerCOAT (Dnr. 20180197) is gratefully acknowledged.

References

[1] L. Berger, Int. Journal of Refractory Metals and Hard Materials Application of hardmetals as thermal spray coatings, RMHM. (2014). doi:https://doi.org/10.1016/j.ijrmhm.2014.09.029.
[2] T. Varis, T. Suhonen, J. Laakso, M. Jokipii, P. Vuoristo, Evaluation of residual stresses and their influence on cavitation erosion resistance of high kinetic HVOF and HVAF-sprayed WC-CoCr coatings, J. Therm. Spray Technol. 29 (2020) 1365–1381, https://doi.org/10.1007/s11666-020-01037-2.
[3] A. Vardelle, C. Moreau, J. Akedo, H. Ashrafizadeh, C.C. Berndt, J.O. Berghaus, M. Boulos, J. Brogan, A.C. Bourtsalas, A. Dolatabadi, M. Dorfman, T.J. Eden, P. Fauchais, G. Fisher, F. Gaertner, M. Gindrat, R. Henne, M. Hyland, E. Irissou, E. H. Jordan, K.A. Khor, A. Killinger, Y.C. Lau, C.J. Li, L. Li, J. Longtin, N. Markocsan, P.J. Masset, J. Matejicek, G. Mauer, A. McDonald, J. Mostaghimi, S. Sampath, G. Schiller, K. Shinoda, M.F. Smith, A.A. Syed, N.J. Themelis, F.L. Toma, J. P. Trelles, R. Vassen, P. Vuoristo, The 2016 thermal spray roadmap, J. Therm. Spray Technol. 25 (2016) 1376–1440, https://doi.org/10.1007/s11666-016-0473-x.
[4] A. Hamilton, A. Sharma, U. Pandel, Solid particle erosion resistance of Hvaf-sprayed Wc-10Co-4Cr coating on Ca6Nm steel, Surf. Rev. Lett. 24 (2017), https://doi.org/10.1142/S0218625X18500117.
[5] B. Huang, C. Zhang, G. Zhang, H. Liao, Wear and corrosion resistant performance of thermal-sprayed Fe-based amorphous coatings: a review, Surf. Coat. Technol. 377 (2019), 124896, https://doi.org/10.1016/j.surfcoat.2019.124896.
[6] X. Luo, R. Chidambaram-Seshadri, G.-J. Yang, Micro-Nanostructured Cermet Coatings, Elsevier Inc, 2019, https://doi.org/10.1016/b978-0-12-813870-0.00004-8.
[7] V. Matikainen, G. Bolelli, H. Koivuluoto, P. Sassatelli, L. Lusvarghi, P. Vuoristo, Sliding wear behaviour of HVOF and HVAF sprayed Cr3C2-based coatings, Wear. 388–389 (2017) 57–71, https://doi.org/10.1016/j.wear.2017.04.001.
[8] Q. Luo, Y.J. Sun, J. Jiao, Y.X. Wu, S.J. Qu, J. Shen, Formation and tribological behavior of AC-HVAF-sprayed nonferromagnetic Fe-based amorphous coatings, Surf. Coat. Technol. 334 (2018) 253–260, https://doi.org/10.1016/j.surfcoat.2017.11.042.
[9] V. Matikainen, K. Khanlari, A. Milanti, H. Koivuluoto, P. Vuoristo, Spray parameter effect on HVAF sprayed (Fe, Cr) C-30FeNiCrSi hardmetal coatings, in: Proc. Int. Therm. Spray Conf, 2016, pp. 184–189.
[10] R.K. Kumar, M. Kamaraj, S. Seetharamu, T. Pramod, P. Sampathkumaran, Effect of spray particle velocity on cavitation erosion resistance characteristics of HVOF and HVAF processed 86WC-10Co4Cr hydro turbine coatings, J. Therm. Spray Technol. 25 (2016) 1217–1230, https://doi.org/10.1007/s11666-016-0427-3.
[11] V. Matikainen, H. Koivuluoto, P. Vuoristo, J. Schubert, Houdková, Effect of nozzle geometry on the microstructure and properties of HVAF-sprayed WC-10Co4Cr and Cr3C2-25NiCr coatings, J. Therm. Spray Technol. 27 (2018) 680–694, https://doi.org/10.1007/s11666-018-0717-z.
[12] C. Lyphout, S. Björklund, M. Karlsson, M. Runte, G. Reisel, P. Boccaccio, Screening design of supersonic air fuel processing for hard metal coatings, J. Therm. Spray Technol. 23 (2014) 1323–1332, https://doi.org/10.1007/s11666-014-0139-5.
[13] A. Ghabchi, Wear Resistant Carbide-based Thermal Sprayed Coatings: Process, Properties, Mechanical Degradation and Wear, PhD Thesis, 2011.
[14] A.J. Sturgeon, Thermal spray technology, 1993.
[15] J.R. Davis, Handbook of Thermal Spray Technology, ASM international, 2004.
[16] S. Matthews, M. Hyland, B. James, Microhardness variation in relation to carbide development in heat treated Cr3C2-NiCr thermal spray coatings, Acta Mater. 51 (2003) 4267–4277, https://doi.org/10.1016/S1359-6454(03)00254-4.
[17] H. Kreye, High velocity oxy-fuel flame spraying-state of art, new developments and alternatives, in: Tagungsunterlagen Conf. Proceedings, Erding 2003, 2003.
[18] L. Jacobs, M.M. Hyland, M. De Bonte, Study of the influence of microstructural properties on the sliding-wear behavior of HVOF and HVAF sprayed WC-cermet coatings, J. Therm. Spray Technol. 8 (1999) 125–132.
[19] Q. Wang, S. Zhang, Y. Cheng, J. Xiang, X. Zhao, G. Yang, Wear and corrosion performance of WC-10Co4Cr coatings deposited by different HVOF and HVAF spraying processes, Surf. Coat. Technol. 218 (2013) 127–136, https://doi.org/10.1016/j.surfcoat.2012.12.041.
[20] P. Matikainen, V. Peregrina, S.R. Ojala, N. Koivuluoto, H. Schubert, J. Houdková, Š. Vuoristo, Erosion wear performance of WC-10Co4Cr and Cr3C2-25NiCr coatings sprayed with high-velocity thermal spray processes, Surf. Coat. Technol. 370 (2019) 196–212, https://doi.org/10.1016/j.surfcoat.2019.04.067.
[21] G. Bolelli, L.M. Berger, T. Börner, H. Koivuluoto, L. Lusvarghi, C. Lyphout, N. Markocsan, V. Matikainen, P. Nylén, P. Sassatelli, R. Trache, P. Vuoristo, Tribology of HVOF- and HVAF-sprayed WC-10Co4Cr hardmetal coatings: a comparative assessment, Surf. Coat. Technol. 265 (2015) 125–144, https://doi.org/10.1016/j.surfcoat.2015.01.048.
[22] A. ASTM, Standard Test Method for Microindentation Hardness of Materials, ASTM Int. West Conshohocken, 2011.
[23] ASTM International, Standard test method for wear testing with a pin-on-disk apparatus G99-17, in: Annu. B. ASTM Stand, 05, 2017, pp. 1–6, https://doi.org/10.1520/G0099-17.Copyright.
[24] ImageJ User Guide User Guide ImageJ, (2012).
[25] M. Randall, Particulate Composites: Fundamentals and Applications, Springer, 2018.
[26] V. Matikainen, H. Koivuluoto, P. Vuoristo, A study of Cr3C2-based HVOF- and HVAF-sprayed coatings: abrasion, dry particle erosion and cavitation erosion resistance, Wear. 446–447 (2020), 203188, https://doi.org/10.1016/j.wear.2020.203188.
[27] G. Bolelli, T. Börner, A. Milanti, L. Lusvarghi, J. Laurila, H. Koivuluoto, K. Niemi, P. Vuoristo, Tribological behavior of HVOF-and HVAF-sprayed composite coatings based on Fe-alloy+ WC–12% Co, Surf. Coat. Technol. 248 (2014) 104–112.
[28] V. Katranidis, S. Gu, B. Allcock, S. Kamnis, Experimental study of high velocity oxy-fuel sprayed WC-17Co coatings applied on complex geometries. Part A: influence of kinematic spray parameters on thickness, porosity, residual stresses and microhardness, Surf. Coat. Technol. 311 (2017) 206–215, https://doi.org/10.1016/j.surfcoat.2017.01.015.
[29] T. Varis, T. Suhonen, M. Jokipii, P. Vuoristo, Influence of powder properties on residual stresses formed in high-pressure liquid fuel HVOF sprayed WC-CoCr coatings, Surf. Coat. Technol. 388 (2020), 125604, https://doi.org/10.1016/j.surfcoat.2020.125604.
[30] K. Torkashvand, V.K. Selpol, M. Gupta, S. Joshi, Influence of test conditions on sliding Wear performance of high velocity air fuel-sprayed WC–CoCr coatings, Materials (Basel). 14 (2021) 3074.
[31] T.B. Torgerson, M.D. Harris, S.A. Alidokht, T.W. Scharf, S.M. Aouadi, R. R. Chromik, Surface & Coatings Technology Room and elevated temperature sliding wear behavior of cold sprayed Ni-WC composite coatings, Surf. Coat. Technol. 350 (2018) 136–145, https://doi.org/10.1016/j.surfcoat.2018.05.090.
[32] M. Surender, B.Ã. Basu, R. Balasubramaniam, Wear Characterization of Electrodeposited Ni – WC Composite Coatings 37, 2004, pp. 743–749, https://doi.org/10.1016/j.triboint.2004.04.003.
[33] I. Baumann, L. Hagen, W. Tillmann, P. Hollingsworth, D. Stangier, G. Schmidtmann, M. Tolan, M. Paulus, C. Sternemann, Process characteristics, particle behavior and coating properties during HVOF spraying of conventional, fine and nanostructured WC-12Co powders, Surf. Coat. Technol. 405 (2021), 126716, https://doi.org/10.1016/j.surfcoat.2020.126716.
[34] A.S.M. Ang, C.C. Berndt, P. Cheang, Deposition effects of WC particle size on cold sprayed WC-Co coatings, Surf. Coat. Technol. 205 (2011) 3260–3267, https://doi.org/10.1016/j.surfcoat.2010.11.045.
[35] C.-J.J. Li, Y.-Y.Y. Wang, G.-J.J. Yang, A. Ohmori, K.A. Khor, Effect of solid carbide particle size on deposition behaviour, microstructure and wear performance of HVOF cermet coatings, Mater. Sci. Technol. 20 (2004) 1087–1096, https://doi.org/10.1179/026708304225019722.
[36] G.C. Ji, X. Chen, H.T. Wang, X.B. Bai, Z.X. Dong, Deformation behaviors of cold-sprayed WC-co particles, J. Therm. Spray Technol. 24 (2015) 1100–1110, https://doi.org/10.1007/s11666-015-0252-0.
[37] P.H. Gao, Y.G. Li, C.J. Li, G.J. Yang, C.X. Li, Influence of powder porous structure on the deposition behavior of cold-sprayed WC-12Co coatings, J. Therm. Spray Technol. 17 (2008) 742–749, https://doi.org/10.1007/s11666-008-9258-1.
[38] V.V. Sobolev, J.M. Guilemany, Flattening of droplets and formation of splats in thermal spraying: a review of recent work - part 1, J. Therm. Spray Technol. 8 (1999) 87–101, https://doi.org/10.1361/105996399770350610.
[39] G.C. Ji, H.T. Wang, X. Chen, X.B. Bai, Z.X. Dong, F.G. Yang, Characterization of cold-sprayed multimodal WC-12Co coating, Surf. Coat. Technol. 235 (2013) 536–543, https://doi.org/10.1016/j.surfcoat.2013.08.021.
[40] P. Chivavibul, M. Watanabe, S. Kuroda, J. Kawakita, M. Komatsu, K. Sato, J. Kitamura, Effects of particle strength of feedstock powders on properties of warm-sprayed WC-Co coatings, J. Therm. Spray Technol. 20 (2011) 1098–1109, https://doi.org/10.1007/s11666-011-9618-0.
[41] P.C. King, M. Jahedi, Relationship between particle size and deformation in the cold spray process, Appl. Surf. Sci. 256 (2010) 1735–1738, https://doi.org/10.1016/j.apsusc.2009.09.104.

[42] C.-J.J. Li, G.-J.J. Yang, Relationships between feedstock structure, particle parameter, coating deposition, microstructure and properties for thermally sprayed conventional and nanostructured WC-Co, Int. J. Refract. Met. Hard Mater. 39 (2013) 2–17, https://doi.org/10.1016/j.ijrmhm.2012.03.014.
[43] U. Nonproportional, C. Loading, J. Appl. Mech. Tech. Phys. 40 (6) (1999) 1126–1132.
[44] C.J. Li, H.L. Liao, P. Gougeon, G. Montavon, C. Coddet, Experimental determination of the relationship between flattening degree and Reynolds number for spray molten droplets, Surf. Coat. Technol. 191 (2005) 375–383, https://doi.org/10.1016/j.surfcoat.2004.04.063.
[45] V.V. Sobolev, J.M. Guilemany, A.J. Martin, Influence of surface roughness on the flattening of powder particles during thermal spraying, J. Therm. Spray Technol. 5 (1996) 207–214, https://doi.org/10.1007/BF02646434.
[46] H.-J. Kim, C.-H. Lee, S.-Y. Hwang, Fabrication of WC–Co coatings by cold spray deposition, Surf. Coat. Technol. 191 (2005) 335–340.
[47] H. Assadi, F. Gärtner, T. Stoltenhoff, H. Kreye, Bonding mechanism in cold gas spraying, Acta Mater. 51 (2003) 4379–4394, https://doi.org/10.1016/S1359-6454(03)00274-X.
[48] C.J. Li, W.Y. Li, H. Liao, Examination of the critical velocity for deposition of particles in cold spraying, J. Therm. Spray Technol. 15 (2006) 212–222, https://doi.org/10.1361/105996306X108093.
[49] C.-J. Li, W.-Y. Li, Y.Y. Wang, H. Fukanuma, Effect of spray angle on deposition characteristics in cold spraying, Therm. Spray 2003 Adv. Sci. Appl. Technol. (2003) 91–96.
[50] H. Wang, X. Yan, X. Liu, H. Lu, C. Hou, X. Song, Z. Nie, Microstructure, mechanical and tribological properties of WC-WCoB coating, J. Eur. Ceram. Soc. 38 (2018) 4874–4881.
[51] K. Kato, Micro-mechanisms of wear—wear modes, Wear. 153 (1992) 277–295.
[52] A. Nieto, J. Kim, O.V. Penkov, D.-E. Kim, J.M. Schoenung, Elevated temperature wear behavior of thermally sprayed WC-Co/nanodiamond composite coatings, Surf. Coat. Technol. 315 (2017) 283–293.
[53] V. Katranidis, S. Kamnis, B. Allcock, S. Gu, Effects and interplays of spray angle and stand-off distance on the sliding wear behavior of HVOF WC-17Co coatings, J. Therm. Spray Technol. 28 (2019) 514–534, https://doi.org/10.1007/s11666-019-00831-x.
[54] J.A.R. Wesmann, S. Kuroda, N. Espallargas, The role of oxide tribofilms on friction and wear of different thermally sprayed WC-CoCr, J. Therm. Spray Technol. 26 (2017) 492–502.
[55] Q. Yang, T. Senda, A. Ohmori, Effect of carbide grain size on microstructure and sliding wear behavior of HVOF-sprayed WC–12% Co coatings, Wear. 254 (2003) 23–34.
[56] Q. Yang, T. Senda, A. Hirose, Sliding wear behavior of WC–12% Co coatings at elevated temperatures, Surf. Coat. Technol. 200 (2006) 4208–4212.
[57] R. Ahmed, O. Ali, N.H. Faisal, N.M. Al-anazi, S. Al-mutairi, F.L. Toma, L.M. Berger, A. Potthoff, M.F.A.A. Goosen, Sliding wear investigation of suspension sprayed WC-Co nanocomposite coatings, Wear. 322–323 (2015) 133–150, https://doi.org/10.1016/j.wear.2014.10.021.
[58] J.M. Guilemany, J.M. Miguel, S. Vizcaino, F. Climent, Role of three-body abrasion wear in the sliding wear behaviour of WC-Co coatings obtained by thermal spraying, Surf. Coat. Technol. 140 (2001) 141–146, https://doi.org/10.1016/S0257-8972(01)01033-7.
[59] J. Jiang, F.H. Stott, M.M. Stack, The Role of Triboparticulates in Dry Sliding Wear 31, 1998, pp. 245–256.
[60] F.H. Stott, G.C. Wood, The influence of oxides on the friction and wear of alloys, Tribol. Int. 11 (1978) 211–218.